User Guide to the CIS measurements in the Cluster Active Archive (CAA)

prepared by

I. Dandouras, A. Barthe

and the CIS Team

DOCUMENT STATUS SHEET

Issue	Date	Details
Version 1.0	30.01.2009	1st version, prepared for the CAA Peer Review. Document referenced as CAA-EST-UG-CIS.
Version 1.1	04.11.2009	Revised version, following recommendations from the CAA Peer Review: • Updated instrument description • Instrument status table added • Updated description of CIS Level 3 data • Updated Data Selection Guide • Section 6.3 added • Other minor updates
Version 1.2	17.05.2010	Various updates, in preparation of the 5th CAA Operations Review.
Version 2.0	29.04.2011	Various updates, in preparation of the 6th CAA Operations Review: • Caveats section reorganised • Appendix added with CIS datasets table • Updated instrument, modes and datasets descriptions • Other minor updates
Version 2.1	27.02.2012	Various updates, including additions of CIS data caveats examples
Version 3.0	10.05.2012	Section added on the CIS data quality indices
Version 3.1	26.07.2012	Various updates
Version 3.2	07.05.2013	Various updates, following the 2013 CIS-CAA Progress Meeting and in preparation of the 8th CAA Operations Review
Version 3.3	13.03.2014	Update in the CIS data quality indices
Version 3.4	09.05.2014	Update in the CIS data quality indices, and various other updates in preparation of the 9th CAA Operations Review
Version 3.5	28.10.2015	Update in the CIS data quality indices, and various other updates.
Version 3.6	12.05.2017	Update in preparation of the 11th CAA Operations Review
Version 3.7	13.06.2017	Update following recommendations of the 11th CAA Operations Review
Version 3.8	11.01.2024	Update following most recent instrument status

TABLE OF CONTENTS

1 Introduction

The CIS (Cluster Ion Spectrometry) experiment is a comprehensive ionic plasma spectrometry package onboard the Cluster spacecraft, capable of obtaining full three-dimensional ion distributions (about 0 to 40 keV/e) with a time resolution of one spacecraft spin (4 sec) and with mass-per-charge composition determination (Rème et al., 2001).

The Cluster Active Archive (CAA) / Cluster Science Archive (CSA) aims at preserving the complete set of the measurements collected by the four Cluster spacecraft, so that they are usable in the long-term by the world-wide scientific community as well as by the instrument team PIs and Co-Is. This implies that the instrument data, properly calibrated, are filed together with the descriptive and documentary elements making it possible to select and interpret them (Perry et al., 2006; Laakso et al., 2010).

This user guide is to provide help to the CAA / CSA user in using the ion observations from CIS. All CIS datasets available in the CAA /CSA are listed in Appendix A.

Note: The term **CAA** is used throughout this document, but it applies equally to the **CSA**.

2 Instrument Description

The CIS package consists of two different instruments:

- a time-of-flight ion *Composition and Distribution Function* analyser (*CODIF*, or *CIS-1*),
- a *Hot Ion Analyser* (*HIA*, or *CIS-2*).

In addition, in order to cover a dynamic range of about 7 orders of magnitude in particle flux, each of the two instruments provides two different geometric factors: a *high-sensitivity side* (or *HS*) for measurements of low ion flux levels (i.e. magnetosphere) and a *low-sensitivity side* (or *LS*) for measurements of high ion flux levels (i.e. solar wind).

Table 2.1 gives the main characteristics of the CODIF and HIA instruments.

2.1 The CODIF (CIS-1) Instrument

The CODIF instrument combines **ion energy per charge selection**, by deflection in a rotationally symmetric toroidal electrostatic analyser, with a subsequent **time-of-flight analysis** after post-

acceleration to ~15 keV/e. Ions are selected as a function of their *E/q* (energy per charge) ratio, by sweeping the high voltage applied between the two toroidal hemispheres. The full energy sweep with 31 contiguous energy channels is performed 32 times per spin, and provides an energy range between about **25 eV/e and 40 keV/e**. In the time-of-flight (TOF) section the velocity of the incoming ions is measured, which allows then the calculation of their *m/q* (mass per charge) ratio. Microchannel plate (MCP) electron multipliers are used to detect both the ions and the secondary electrons, which are emitted from a carbon foil at the entry of the TOF section, during the passage of the ions. These secondary electrons give the "START" signal, for the time-of-flight measurement, and the position information (elevation angle of the incoming ion, provided by the MCP sectoring in anodes), cf. Fig. 2.1. The "STOP" signal, for the time-of-flight measurement, is provided by the ion detection at the MCP.

CODIF consists of **two sections**, each with a 180° field of view, with geometry factors differing by a factor of ~ 100: two different entrance grids are used (one per section), to reduce the incoming flux. This way, one of the sections will have counting rates which are statistically meaningful and which at the same time can be handled by the time-of-flight electronics. However, intense ion fluxes can in some cases saturate the CODIF instrument (particularly if data are acquired from the high sensitivity side), but these fluxes are measured with HIA, which is less sensitive to saturation (for examples, see section 6). The operation of the **high-sensitivity side** ("high-G", or "HS") and of the **low-sensitivity side** ("low-g", or "LS") on CODIF is **mutually exclusive**, and only one of the two sides can be selected at a time to supply data. There are eight 22.5° sectors (or anodes) in the HS side, and six 22.5° sectors in the LS side. Note that the latter has two "blind" anodes (parallel and anti-parallel to the spin axis). The field of view of the CODIF anodes is shown in Figure 2.2.

With an additional **Retarding Potential Analyser (RPA)** device in the aperture system of the CODIF sensor, and with pre-acceleration for the energies below 25 eV/e, the range is extended to energies as low as the spacecraft potential. The retarding potential analyser operates only in the RPA mode, and provides an energy range between about 0.7 and 25 eV/e (with respect to the spacecraft potential). The RPA aperture system has a geometric factor which is the same for either of the two CODIF sensitivity sides.

2.2 The HIA (CIS-2) Instrument

The HIA instrument is an ion energy-spectrometer, capable of obtaining full three-dimensional ion distributions with good angular and time resolution (one spacecraft spin). HIA combines the selection of incoming ions, according to the **ion energy per charge** by electrostatic deflection in a

quadrispherical analyser, with a fast imaging particle detection system. This particle imaging is based on microchannel plate (MCP) electron multipliers and position encoding discrete anodes. As for CODIF, ions are selected as a function of their *E/q* (energy per charge) ratio, by sweeping the high voltage applied between the two hemispheres, cf. Fig. 2.3. However, with no TOF section, the ion mass cannot be resolved by HIA. The instrument has 62 energy channels but this is then reduced on-board to a lower number (mode dependent), by binning together adjacent channels, to fit into the allocated telemetry.

HIA consists of two 180° field-of-view sections, with two different sensitivities (with a ~20 ratio), corresponding respectively to the **high-sensitivity** ("high-G", or "HS") and to the **low-sensitivity** ("low-g", or "LS") side. The "low g" side allows detection of the solar wind and the required high angular resolution is achieved through the use of 8 sectors (or MCP anodes) around the spin plane, 5.625° each, the remaining 8 sectors having an 11.25° resolution. The 180° "high G" side is divided into 16 sectors, 11.25° each. For each sensitivity side a full 4π steradian scan, consisting of 32 energy sweeps, is completed every spin of the spacecraft, i.e. every ~4 s, giving a full three-dimensional distribution of ions in the energy range **~5 eV/e - 32 keV/e**. The field of view of the HIA anodes is shown in Figure 2.4.

HIA and CODIF are thus complementary instruments: ion composition and coverage of the high-energies (32-40 keV/e) are provided only by CODIF, whereas HIA provides a higher angular and energy resolution. HIA is also less prone to saturation: it does not saturate in the LS side, but the HS side can occasionally saturate. **In section 6 a table is provided to help the user select the most suitable instrument,** depending on the region and the ion population analysed.

Figure 2.5 shows representative ion fluxes encountered along the Cluster orbit.

Sensor	Energy Range	Energy Resolution (FWHM)	Time Resolution		Mass Resolution M/ΔM	Angular Resolution	Dynamics $(cm^2\ sec\ sr)^{-1}$
			2D ms	3D s			
HIA	~ 5 eV/q - 32 keV/q	18%	62.5	4	-	~ 5.6° x 5.6°	10^4 - 2 x 10^{10}
CODIF	~ 0 - 40 keV/q Mass range: 1 - 32 amu	16%	125	4	~ 4 - 7	~11.2° x 22.5°	3×10^3 - 3×10^9

Sensor	Full Instantaneous Field of View	Geometrical Factor (Total) $cm^2.sr.keV/keV$	Mass	Power (Nominal Operations)
HIA	8° x 360°	7.0 x 10^{-3} for the HS half 3.7 x 10^{-4} for the LS half	2.45 kg	2.82 watts
CODIF	8° x 360°	1.9 x 10^{-2} for the HS half 2.1 x 10^{-4} for the LS half 3.0 x 10^{-2} cm^2 sr for the RPA	8.39 kg	6.96 watts

Table 2.1. Main characteristics of the CIS Experiment

3 Instrument Operations

3.1 The CIS Operational Modes

The CIS instruments have a large amount of flexibility either in the selection of the operational mode or in the reduction of the data necessary to fit the available telemetry bandwidth. CIS can thus operate in any combination of the 6 Spacecraft Telemetry Modes (3 Normal Telemetry Modes, NM1-NM3, and 3 Burst Telemetry Modes, BM1-BM3) and the 16 CIS Operational Modes. For further details on spacecraft modes, see Laakso (2012).

CIS Mode		Mode Name
0	SW-1	Solar Wind / SW tracking - Mode 1
1	SW-2	Solar Wind / 3D upstreaming ions - Mode 2
2	SW-3	Solar Wind / SW tracking - Mode 3
3	SW-4	Solar Wind / 3D upstreaming ions - Mode 4
4	SW-C1	Solar Wind / SW tracking - Data Compression - Mode 1
5	SW-C2	Solar Wind / 3D upstreaming ions - Data Compression- Mode 2
6	RPA	RPA Mode
7	PROM	PROM Operation
8	MAG-1	Magnetosphere - Mode 1
9	MAG-2	Magnetosphere - Mode 2
10	MAG-3	Magnetosphere - Mode 3
11	MAG-4	Magnetosphere / Magnetosheath - Mode 1
12	MAG-5	Magnetosheath - Mode 2
13	MAG-C1	Magnetosphere - Data Compression - Mode 1
14	MAG-C2	Magnetosheath - Data Compression - Mode 2
15	CAL	Calibration / Test Mode

Table 3.1. CIS Operational Modes. Their characteristics (that vary between NM and BM) are explained in Rème et al (2001).

These 16 modes (Table 3.1) can be grouped into solar wind tracking modes, solar wind study modes with the priority on the upstreaming ions, magnetospheric modes, magnetosheath modes, an RPA mode, a calibration and test mode, and a PROM operation mode (instrument check-out). These modes correspond to different energy sweeping schemes and different combinations of telemetry products transmitted.

The calibration and test mode and the PROM operation mode do not generate any science data to be archived at the CAA. However, the PROM mode generates an uncalibrated “raw counts” data product.

On-board calculated moments are always transmitted to the telemetry with a high-time resolution (1 spin). A combination of 2-D and 3-D ion distribution functions, plus other telemetry products, are transmitted in parallel to on-board calculated moments, with a mode-dependent and product-dependent time resolution. Mode change is performed by time-tagged commands, according to the predicted plasma populations anticipated along the Cluster orbit.

Although during the first two years of operations (2001-2002) various CIS mode selection rules have been in use, since 2003 the modes have been applied in the following manner.

- Magnetosphere:
  - most common: Mode 8 (MAG-1) and 13 (MAG-C1)
  - Mode 10 (MAG-3) is also used in the magnetosphere for providing full resolution HIA data at the expense of CODIF data, as e.g. onboard sc1 since the end of 2004, when CODIF failed on this spacecraft (cf. section 3.2)
  - RPA Mode: it is operated about once per month, either on all spacecraft or on selected spacecraft
- Magnetosheath:
  - most common: Mode 12 (MAG-5) and 14 (MAG-C2)
- Solar wind:
  - most common: Mode 3 (SW-4) and 5 (SW-C2)

3.1.1 Magnetospheric Modes (Modes 8 - 11, 13)

They are relatively simple modes, i.e. the **full energy-angle ranges are systematically covered**. For HIA the different telemetry products (including moments) are deduced from the 62E x 88Ω energy-solid angle count rate matrices accumulated on the "high G" section, and eventually reduced to a lower energy resolution by binning together adjacent channels. For CODIF they are deduced from the sensitivity side selected by command and from a similar energy-solid angle matrix as for HIA and similarly eventually reduced to a lower energy resolution.

3.1.2 Solar wind tracking modes (Modes 0, 2, 4)

They allow a precise and fast measurement (4 s) of the ion flow parameters (H^+, He^{++}). For that, in the solar wind, for HIA the energy sweep range is automatically reduced when the field-of-view of the LS side is facing the 45° sector centred in the solar wind direction. This **energy sweep range** is adapted every spin, **centred on the main solar wind velocity** by using a criterion based on the H^+ thermal and bulk velocities computed during the previous spin (solar wind beam tracking). This allows a

higher energy resolution for the solar wind beam data and more accurate ion moments of the solar wind.

3.1.3 Solar wind / upstreaming ions modes (Modes 1, 3, 5)

In these modes solar wind beam tracking is performed by HIA only once every ~16 spins (exact value can vary depending on mode number). During the remaining 15/16 spins a broader energy sweep is used for the solar wind detection by the LS side, allowing at the same time the detection of upstreaming ions by the HS side, which is then looking in the anti-sunward direction. Detailed 3-D distributions for the solar wind (LS side) are then transmitted to the telemetry only during solar wind beam tracking (once every ~16 spins), but onboard calculated solar-wind moments are transmitted every spin. Moreover, detailed 3-D distributions from the HS side (e.g. for upstreaming ions and/or for interplanetary disturbances) are included in the basic products transmitted to the telemetry.

Outside this 45° sector, the full energy sweep range is used (**solar wind tracking modes and solar wind modes with the priority on the upstreaming ions, i.e. modes 0 - 5**). However, when the field-of-view of the HS side is facing the 45° sector centred in the solar wind direction (cf. Fig. 3.1), the energy sweep stops (and "freezes") above the solar wind alpha particles energy, to avoid a quick degradation of the MCPs by the intense solar wind beam (modes 0 - 5).

For CODIF, the reduced energy-sweep principle is also used during modes 0 - 5, when the field-of-view of the HS side section is facing the 45° sector centred in the solar wind direction. Complete energy sweeping is used in the remaining part of the spin (Fig. 3.2).

3.1.4 Magnetosheath modes (Modes 12, 14)

These modes are like magnetospheric modes. However, starting from 1 November 2003, the energy sweep scheme has been redefined for CODIF. With the new CODIF Magnetosheath Modes (modes 12 and 14), the energy sweeps are truncated and "frozen" at about 2 keV for 16 out of 32 sweeps (when the HS side faces the magnetosheath mainstream flow), to save the MCP lifetime.

3.1.5 RPA mode (Mode 6)

When the RPA mode is selected, **CODIF** operates exclusively in the **0.7 - 25 eV/e energy range** of the retarding potential analyser, whereas HIA operates as during magnetospheric modes, cf. section 3.1.1 (full energy coverage).

3.1.6 PROM mode (Mode 7)

PROM mode is activated during instrument switch-on, before selecting another operational mode. However, in case of failure of using the instrument EEPROM memory, PROM mode is the only operational mode. This has been the case for the HIA instrument onboard Cluster-1 since 5 February 2021. In this case the only ion count data transmitted is a diagnostic product, consisting of the raw ion counts organised in 32 energy bins x 48 solid angles. Each of these data records corresponds to a 2D "snapshot" of the ion distribution, acquired over one energy sweep.

Information on the selected CIS operational mode and instrument sensitivity side is given in the CIS-MODES dataset. It is also repeated, for convenience, in the "cis_mode" and "sensitivity" record varying variables of the various datasets.

Caveat: The example discussed in section 6.3 illustrates the influence that an inappropriate mode selection can have in the CODIF and HIA data when using HIA LS/HS side and/or CODIF LS/HS side data in a wrong region (e.g. HS side in the solar wind).

3.2 CIS Instrument Status

The overall experiment performance, after about 23 years of operation in space, is good. The particle detection efficiency degradation, due to the MCP gain fatigue mechanism (Prince and Cross, 1971), is moderate for the HIA instrument. For CODIF the efficiency degradation is more pronounced, due to the operational principle of this instrument, requiring the detection of both the ion ("stop" time-of-flight signal) and of the electrons emitted by the carbon foil ("start" time-of-flight signal), plus a "position" signal, to validate the detection of an ion. When processing the raw instrument data to convert them into higher-level data in physical units, these efficiency degradations are compensated by the calibration values used, supplied in the calibration files (cf. Section 4). Table 3.2 gives a summary of the CIS instrument status.

Cluster 1: The **CODIF** instrument is switched off since 25 October 2004, due to an MCP high voltage anomaly. The **HIA** instrument operations, since April 2011, have been restricted to magnetospheric modes only and since November 2012 the duration of operations is also limited to 1 hour per orbit, (and up to 2 x 1 hour per day since December 2016), becoming even shorter later, due to an issue related to the ageing of the analyser sweep high-voltage supply system. Since 5 February 2021 the instrument has been operating in PROM mode only, due to a failure in an electronic component. Since January 2024 the HIA instrument onboard Cluster 1 has not been switched-on any more, due to limitations in the spacecraft power supply.

Cluster 2: The CIS experiment is not operational.

Cluster 3: The CIS experiment has been operating nominally until the 11 November 2009 when, during normal operations, it was switched-off by the spacecraft onboard monitoring. Analysis provides evidence for a damaged electronic component, after having operated several times the design lifetime of 2 years and after having received several times the design total radiation dose. The CIS experiment, onboard this spacecraft, is considered as not operational any more.

Cluster 4: The **HIA** instrument is switched off. On this spacecraft, due to an electrostatic analyser high voltage issue, the HIA energy sweep range is limited between ~5 eV/e and ~400eV/e.

Table 3.2 gives a summary of the CIS instrument status.

	SC 1	SC 2	SC 3	SC 4
CODIF	Operations until 25 Oct. 2004	Not Operational	One deficient MCP quadrant (cf. section 6.2), until switch-off on 11 Nov. 2009	Normal operations
HIA	Normal operations. Magnetospheric modes only since Apr. 2011. Operations reduced to 1 hour segments since November 2012. PROM mode only since February 2021. Switched-off since January 2024.		Normal operations until 11 Nov. 2009	Not operational so-far (switched OFF due to reduced energy coverage)

Table 3.2. Summary of CIS Instrument Status

4 Measurement Calibration and Processing procedures

Both CODIF and HIA have been very well calibrated before launch, in vacuum test facilities (Rème et al., 2001). However, due to the in-flight evolution of the MCP detection efficiencies as a function of time, the CIS calibration files are updated regularly. A calibrations catalogue file, which is provided with the calibration files, serves as a pointer to which calibration files to use for each data time period. This catalogue file evolves in an incremental way through the mission, to take into account the existence of new calibration files, which correspond to the instrument particle detection efficiency evolution, or other changes in the instrument.

Calibration files include thus parameters that have been determined during ground calibrations in vacuum test facilities and are stable through the mission (e.g. instrument angle response, electrostatic analyser constant used in the calculation of the energy sweep tables, etc.), parameters that change gradually through the mission (e.g. particle detection efficiencies), and parameters that can be changed during the mission by command (e.g. upload of new spin accumulation tables for 3-D ion distributions in the various modes). All of them are equally important in converting raw data into physical units, and are used together.

The in-flight calibration procedure is described in Kistler et al. (2013) and in Blagau et al. (2014), for the CODIF and HIA instruments respectively.

How the calibration values are used to convert particle raw counts in physical units, such as particle flux, or moments of the ion distribution functions, is described in the Appendix of the CAA-CIS Interface Control Document (Dandouras and Barthe, 2013).

A CIS Calibration Report is also provided by the CIS team to the CAA (Dandouras et al., 2013).

The CIS calibration files will be archived at the CAA.

5 Key Science Measurements and Datasets

For the archival of the CIS data a multi-level approach has been adopted. The CAA archival includes processed raw data (not delivered yet), moments of the distribution functions, calibrated high-

resolution data in a variety of physical units, and a number of ancillary datasets. Furthermore, the calibration files and high-level processing software are also archived. For details of all CIS products in the CAA, cf. the CAA-CIS Interface Control Document (Dandouras and Barthe, 2013).

5.1 Ion moments

The CIS moments of the particle distribution functions include: ion density, velocity, temperature (parallel and perpendicular to the magnetic field components), and pressure.

There are two kinds of moments available on the CAA: those produced onboard and those produced on the ground. On-board calculated moments and on ground calculated moments are complementary as the onboard moments have better time resolution while ground moments have better calibration values. The calculations of the moments of the 3-D ion distribution functions are described in the Appendix of the CIS-CAA ICD (Dandouras and Barthe, 2013).

5.1.1 On-board moments

The HIA onboard calculated moments correspond to the Prime Parameters from the Cluster Science Data System (Daly et al., 2002): on-board calculated moments with 1-spin resolution and calculated from the full angular and energy resolution 3-D ion distributions, then reprocessed on ground (total efficiency calibration adjustments, coordinate transformations etc.). However, the FGM CAA spin-resolution data are here used for calculating parallel and perpendicular ion temperatures. In addition, the ion velocity is provided in both GSE and ISR2 reference frame, and the whole pressure tensor in ISR2 is included.

5.1.2 Ground moments

In addition to the on-board calculated moments, CIS data include also CODIF moments calculated on ground from the 3-D ion distributions: H^+, He^+ and O^+. These provide better calibration adjustments (per anode efficiency) and are thus more accurate, but have a reduced time and energy resolution. CODIF ground calculated moments are based on energies above 28 eV, so all low-energy ions are excluded.

HIA on ground calculated moments are not supplied, because the same anode calibrations would be used as for the on-board calculated ones, but with a degraded time, energy and angular resolution (no added value).

A software package has also been developed and is available for download at the CAA web site, allowing the user to interactively calculate partial (or total) moments of the ion distributions, for selected energy and solid angle ranges: CODIF (all 4 ion species) and HIA data (cf. section 5.4).

On-board calculated moments and on ground calculated moments from the 3-D ion distributions are thus complementary (cf. section 6.1, data selection guide).

5.2 Ion distribution functions

The 3-D ion distributions are produced by correcting the raw data for detector efficiencies, geometric factors and other information available from the calibration tables, and give measurements in several physical units (in separate files):

- (differential) particle flux (ions cm^{-2} s^{-1} sr^{-1} keV^{-1})
- particle energy flux (keV cm^{-2} s^{-1} sr^{-1} keV^{-1})
- particle phase space density (ions s^{3} km^{-6})
- corrected-for-efficiency particle count rate (ions s^{-1})
- raw particle counts (number of ions per counter bin)

These datasets are constructed by joining data of the same ion species from different modes that can have different angular, energy or time resolution, in order to create a single dataset per ion species and per sensitivity type (LS/HS). When data from modes with different energy (or angular) resolution are joined into a single dataset, the highest available energy (or angular) resolution is retained whereas data from the lower resolution mode have their ion counts, of each energy (or solid angle) bin, splitted equally into two bins to fit the higher resolution format.

5.2.1 3D ion distribution functions

The 3-D ion distributions are given in the ISR2 pseudo-GSE reference frame (X sunward, Z is the spacecraft axis and northward pointing), see Laakso (2012). They give the complete 16 azimuth × 8 elevation = 128 solid angles matrix, and remove the reduction to a total of 88 solid angles in the telemetry products, where adjacent solid angles near the polar directions have been binned together (for some CIS telemetry products). Solid angles, defined in the distributions, correspond to particle arrival directions (direction of travel of the particle). This implies that:

- Phi is the azimuth angle. In the ISR2 reference frame phi = 0° for a particle travelling sunward and phi = 90° for a particle travelling duskward.

- Theta is in the polar angle. In the ISR2 reference frame theta = 90° for a particle travelling along the Northward Z- axis.

5.2.2 Pitch-angle ion distribution functions

In addition to the 3-D distributions, pitch-angle distributions (PADs) are also provided. These are calculated on ground from the 3-D distributions and the magnetic field direction (spacecraft reference frame), are given only in particle flux units as a function of the particle energy and pitch-angle (2-D distributions), and their resolution is in 16 angular sectors covering the pitch angle range from 0° to 180°. It is noted that the data from the full 3-D distributions are used in generating the PADs, and not just a 2-D "cut" in the plane containing the magnetic field vector.

5.2.3 Omni-directional ion distribution functions

Omni-directional fluxes (1-D ion distributions as a function of energy, in particle energy flux units) constitute another CIS archived dataset, which provides an overview of the plasma environment.

5.3 CIS Graphical Data Products

The CIS graphical data archived are 6-hour energy-time ion spectrograms. They are pre-formatted displays: PNG graphic files embedded in HTML pages, and they are given at two levels of resolution: browsing and detailed. These spectrograms are supplied separately for each spacecraft. They are also available at http://cluster.irap.omp.eu/public/spectro/index.php?vue=SCI.

5.4 CIS Data Processing Software

The CIS data processing software delivered to the CAA contains two packages:

- ***CIS_3D_MOM* software**: specially developed for the CAA, allows the user to interactively calculate partial or total moments of the ion distributions, for selected energy and solid angle ranges. The necessary input is 3-D ion distribution files, in CEF-2 format and in corrected-for-efficiency particle count rate units, available at the CAA. The output parameters are ion density, bulk velocity, pressure tensor and temperature, also in CEF-2 format and in the ISR2 reference frame. It is written in C and it can be used for either CODIF or HIA data. It can be downloaded from the CAA software webpage.

- ***cl* software**: it is written in IDL, and developed initially for the CIS team. It reads raw CIS data and CIS calibration files; is interactive, and can generate a large variety of high-resolution graphics (spectrograms, distribution functions, PADs …) in several physical units. It can also export the results as ASCII (CEF) data files. In addition to the CIS data, this software can also read generic CDF

and CEF data files, for correlation studies. For the *cl* software, the user can contact Emmanuel.Penou@irap.omp.eu.
A web-based version of the *cl* software has also been developed, called *clweb*, and is available at http://clweb.irap.omp.eu/.

These software packages, *CIS_3D_MOM* and *cl*, are available "as documents", for installation and execution on the end user's machine.

5.5 CIS Data Caveats

Given the complexity of an ion spectrometer, and the variety of its operational modes, each one being optimised for a different plasma region or measurement objective, consultation of the data caveats by the end user will always be a necessary step in the data analysis (independently of the data level).

An internal caveats database, containing instruments caveats for the whole mission, is available at http://cluster.irap.omp.eu/index.php?page=caveats&langue=en. This database has been also delivered to the CAA.

The caveats are automatically delivered together with the requested datasets to the user if there are caveats for the requested time interval.

Commanding issues :

- **Operation incidents** : They can occasionally result, for short periods, in missing data products, in incorrect MCP high voltage and/or discriminator settings, which reduce the accuracy of the collected data, etc. These are flagged in the caveats for specific data intervals.
- **Data acquired during instrument mode switches** : should be used with caution (+/- up to 2 spins from mode change).

Cf. section 6.2 of this document for the main CIS data caveats. Note that these caveats are not included in this caveat dataset.

5.6 CIS Data Quality Indices and Flags

CIS data quality indices are given in five datasets, one for the HIA data and one for each of the four major ion species detected by CODIF (H^+, He^{++}, He^+, O^+).

For each dataset, **four separate data quality indices** are given, i.e. one for each of the four CIS dataset families:

- Moments (CODIF ground calculated moments and HIA onboard moments)
- 3-D distributions
- Pitch-angle distributions (PAD)
- Omni-directional fluxes (1-D)

These CIS data quality indices are based on the CAA standard (as revised by the 58th SOWG):

- **0** : Not applicable (used by CIS to flag no science data tacking periods)
- **1**: Major problems, check caveats
- **2**: Minor problems, check caveats
- **3**: Good data (default CIS data quality index value, unless a data quality issue is identified, degrading the quality index value).
- **4**: Excellent data which has received special treatment.

Moreover, the **-1** data quality index value is used in order to identify scientifically unusable data, to be removed from the CIS datasets.

In each CIS data quality record, **in addition to the four data quality indices** (one for each of the four CIS dataset families), and if the value of at least one of the indices is less than 3 (inadequate data quality), a **CIS-specific flag** (caveats_key) is also included. This flag is an ASCII string that refers to the **type of caveat** that affects the quality of the data. Eventually more than one such flags may be given, if several issues affect the quality of the data.

The **list** of the CIS-specific flags (caveats_keys) is given in **Appendix B**.

A description of the relevant caveats is given in **section 6.2** of this User Guide, including examples of data affected by these issues.

6 Recommendations

6.1 CIS Data Selection Guide

Table 6.1 provides a CIS data selection guide for the CAA user: which CIS datasets are the most suitable, depending on the region and the ion population analysed.

- "1st priority" indicates the most suitable datasets. Following priorities indicate data that can be used if the "1st priority" data are not available (e.g. mode not selected, instrument OFF etc.), but can be less accurate, as explained in the caveats.

- Text in gray indicates partial moments data that the user can calculate for the ion population under study, e.g. calculating the density and the velocity of an ion beam propagating within a denser ambient plasma. This requires running the partial moments software by the user (cf. Section 5.4).

Table 6.1. Guide for selecting the right CIS dataset in different regions

Region or ionic plasma population	Ion moments	Ion distribution functions
Solar wind (solar wind beam)	▪ 1st priority: HIA / SW modes / onboard calculated moments ▪ 2nd priority: CODIF / LS side / SW modes / ground calculated moments ▪ 3rd priority: HIA / MAG modes / onboard calculated moments (partial saturation) ▪ 4th priority: CODIF / LS side / MAG modes / ground calculated moments (interference from the HS side)	▪ 1st priority: HIA / LS side / SW modes ▪ 2nd priority: CODIF / LS side / SW modes ▪ 3rd priority: HIA / HS side / MAG modes (partial saturation) ▪ 4th priority: CODIF / LS side / MAG modes (interference from the HS side)
Solar wind foreshock region : upstreaming ions	▪ 1st priority: HIA / HS side / SW or MAG modes / partial moments ▪ 2nd priority: CODIF / HS side / SW modes / partial moments ▪ 3rd priority: CODIF / HS side / MAG modes / partial moments (interference from the solar wind) Note: these can be obtained only by running the partial moments software (cf. 5.6)	▪ 1st priority: HIA / HS side / SW or MAG modes ▪ 2nd priority: CODIF / HS side / SW modes ▪ 3rd priority: CODIF / HS side / MAG modes (interference from the solar wind)

Magnetosheath	▪ 1st priority: HIA / MAG modes / onboard calculated moments ▪ 2nd priority: CODIF / LS side / MAG or MSH modes / ground calculated moments	▪ 1st priority: HIA / HS side / MAG modes ▪ 2nd priority: CODIF / LS side / MAG or MSH modes
Cusp	▪ 1st priority: HIA / MAG modes / onboard calculated moments ▪ 2nd priority: CODIF / LS or HS side / MAG modes / ground calculated moments	▪ 1st priority: HIA / HS side / MAG modes ▪ 2nd priority: CODIF / LS or HS side / MAG modes
Outer Magnetosphere (including plasma sheet)	▪ 1st priority: CODIF / HS side / MAG modes / ground calculated moments ▪ 2nd priority: HIA / MAG modes / onboard calculated moments (can miss higher energy particles)	▪ 1st priority: CODIF / HS side / MAG modes ▪ 2nd priority: HIA / HS side / MAG modes (can miss higher energy particles)
Magnetosphere: ion beams (e.g. PSBL)	▪ 1st priority: CODIF / HS side / MAG modes / partial moments ▪ 2nd priority: HIA / MAG modes / partial moments	▪ 1st priority: CODIF / HS side / MAG modes ▪ 2nd priority: HIA / HS side / MAG modes
Inner Magnetosphere: Ring Current population	▪ CODIF / HS side / MAG modes / ground calculated moments	▪ CODIF / HS side / MAG Modes
Inner Magnetosphere: Plasmashereric population	▪ CODIF / RPA Mode / partial moments	▪ CODIF / RPA Mode

HS : High-sensitivity instrument side

LS : Low-sensitivity instrument side

SW modes : Solar wind modes

MAG modes : Magnetospheric modes

MSH modes : Magnetosheath modes

RPA mode : Retarding Potential Analyser mode

6.2 CIS Data Caveats

Note that the caveats in this section are not given in the caveat dataset but these are observational limitations which the user should be aware of when analysing CIS observations

6.2.1 Only partial moments measured

- **Limited energy range**: The calculated density values are in reality ion partial density values in the energy domain covered by the instrument, typically 25 eV/e to 40 keV/e for CODIF and 5 eV/e to 32 keV/e for HIA. In the presence of cold plasma at energies below the instrument energy threshold, or of hot plasma at energies above the instrument upper energy limit, this partial density is evidently lower than the total plasma density. In the presence of hot plasma at energies above the instrument upper energy limit the result is also underestimated ion bulk velocity, temperature and pressure values.

- **Positive spacecraft potential:** The instrument energy domain is always defined with respect to the spacecraft potential. Spacecraft charging to a high positive floating potential, as can be the case in low density plasmas when the ASPOC ion emitter for spacecraft potential control is not operating (Torkar et al., 2001), repels the low-energy ions which in these cases cannot be detected by CIS (cf. for example section 6.10 of Rème et al., 2001, and section 3.4 of Dandouras et al, 2005). This effect results in a further increase of the difference between the partial density, measured by CIS, and the total plasma density. Figure 6.1 provides such an example.

6.2.2 Limitations related to sampling of ion distributions

- **Limited energy/angular resolution:** In addition to the finite energy range, the accuracy of the computed moments is also affected by the finite energy and angular resolution of the two instruments. This is in particular the case for narrow-energy distributions (cold plasmas or cold beams), and/or narrow solid angle beams. CODIF is more sensitive to this effect, due to its coarser energy and angular resolution.

- **Poor counting statistics**: Adequate counting statistics are essential for reliable results. For density calculations, in the case of isotropic plasma distributions, HIA "hits" a lower limit density value of the order of 0.01 - 0.02 cm^{-3}. CODIF continues to supply density values down to about 0.001 - 0.002 cm^{-3}, although with very poor counting statistics in these cases, which do not allow a reliable calculation of the higher-order moments (velocity, temperature and pressure). Fig. 6.2 gives an example of such data, acquired in the magnetospheric lobes.

- **Solar wind modes:** The entire velocity phase space, corresponding to the instrument energy domain, is not covered during all modes (cf. section 3.1 and for an example cf. the spectrogram discussed in section 6.3). This is the case during solar wind modes, and during some magnetosheath modes (CODIF data acquired after1 November 2003 during modes 12 and 14). The result is:

    - Incorrect HIA moment values in the magnetosheath when the instrument is in a solar wind mode (modes 0-5).
    - Incorrect CODIF moment values when data come from the high-sensitivity side and the instrument is in a solar wind mode (modes 0-5).
    - Incorrect CODIF moment values when data come from the high-sensitivity side and the instrument is in mode 12 or 14, for data acquired after1 November 2003.

- **Eclipses:** During short eclipses (intervals are given in the quality index files) the absence of a Sun reference pulse completely desynchronises the HIA data, which become useless, whereas the CODIF data are acquired using an extrapolated Sun reference pulse, and some of the CODIF data can be used. However, any directional data are not useable. During long eclipses CIS is off.

6.2.3 Errors due to onboard data compression and incomplete data transmission

- In order to transmit the full 3D distribution, while overcoming the telemetry rate limitations, a compression algorithm has been introduced, which allows an increased amount of information to be transmitted. This however does not always work well in all situations, and partial data loss can sometimes occur (partial data gaps), which can eventually result also in a sampling alias effect on the transmitted values. When sampling becomes irregular due to the data compression, also the actual moments may become less reliable. Figure 6.3 provides such an example. Most of such intervals are flagged in quality indices.

6.2.4 Detector saturation, contamination issues

- **Detector saturation:** Ion measurements are sensitive to eventual detector saturation in the presence of high ion fluxes (instrument dead time effects). The most striking example is the strongly underestimated solar wind density and magnetosheath density by the CODIF high-sensitivity side, while the instrument is operating in a magnetospheric mode (cf. example given in section 6.3). However, these saturation effects are phase space dependent: the detector can be saturated only in a limited energy range and for particles arriving in a given solid angle, where the highest counting rates occur (e.g. solar wind beam), but at the same time can supply reliable measurements in the remaining phase space. Note that HIA data acquired in a magnetospheric mode can also suffer from partial detector saturation when in the solar wind: slightly underestimated densities, by a factor depending on the solar wind density and temperature (Martz et al., 1993).

- **Background noise:** Eventual instrument background counts due to penetrating particles, from the radiation belts around perigee passes or during SEP (Solar Energetic Particles) events, can result in an overestimation of the measured fluxes, and the resulting density values. This effect is stronger for HIA, whereas for CODIF it is mitigated by the time-of-flight technique, which requires both a “start” signal and a “stop” signal, in the correct time-of-flight window, to validate the detection of an ion. However, in the harsh environment of the inner radiation belt, even CODIF suffers from such a background. Figure 6.4.a shows an example of background induced on the HIA (top panel) and CODIF (bottom panel) ion counting statistics, due to penetrating particles from the radiation belts, outer and inner (Ganushkina et al., 2011). Figure 6.4.b shows an example of

background induced on the HIA ion counting statistics, while in the solar wind, due to the arrival of Solar Energetic Particles during an extreme solar event.

- **Cross-talk:** CODIF data in the solar wind, if acquired from the LS side but with the instrument operating in a magnetospheric mode, can suffer from cross-talk with the high counting rates of the HS side, which is then saturated by the solar wind. Note that both sensitivity sides simultaneously collect data, even if only one sensitivity side is selected at any time for data transmission. The result is then overestimated densities and underestimated velocities. Figure 6.5 shows such an example.

- **Ion species spillover and He^{++} contamination**: CODIF mass-separated data can suffer from spillover between neighboring mass channels (Kistler, 2000). He^{++} data, in particular, are usually contaminated by H^+ ions, resulting in over-estimated He^{++} densities. Therefore the He^{++} moments are not given in the CAA. The He^{++} fluxes are archived but the user should be aware of a strong H^+ contamination in these data.

- **O^+ contamination:** CODIF O^+ data can be contaminated by penetrating particles in the radiation belts. They can also be contaminated by H^+ ions in very high H^+ flux plasmas, as for example in the magnetosheath. The latter is due to occasionally two uncorrelated H^+ ions, one generating only a "start" time-of-flight signal and the other generating only a "stop" time-of-flight signal, and the time difference between the two being that of an O^+ ion. Figure 6.6 gives an example of such a contamination of O^+ data from very high H^+ fluxes.

- **Ion species effects on HIA:** Presence of ion species other than H^+ in the HIA data results in underestimated densities and in overestimated temperatures and pressures.

6.2.5 Calibration issues

- **Inter-anode calibration errors** : The V_z term of the ion bulk velocity is very sensitive to the anode cross-calibrations, and in particular to those of the anodes looking in directions away from the spacecraft spin plane (polar anodes). In some cases the efficiency calibration coefficients cannot completely compensate for strongly asymmetrically decreased efficiencies of such polar anodes, which results in a residual offset of V_z .

CODIF on Cluster 3: One MCP quadrant (southward looking directions on the high-sensitivity side) suffers from a strongly decreased particle detection efficiency. This asymmetric efficiency degradation is amplified with time. For data acquired up to 23 February 2003 the effect has been corrected; after this date it cannot anymore be corrected. As a result the V_z velocity component is highly unreliable (strong offset), and the density suffers from the fact that the instrument under-detects the ions in one hemisphere of the phase space.

- **Detector ageing**: It is accompanied by a degradation of the signal-to-noise ratio (reduced counting statistics).
- **Calibrations accuracy**: Determinations of the evolution of the MCPs detection efficiency are statistical.

6.3 Example of the influence on the data of an inappropriate mode selection

The energy-time ion spectrogram, shown in Fig. 6.7, gives an example illustrating the influence that an inappropriate mode selection can have in the CODIF and HIA data, when using HIA LS/HS side and/or CODIF LS/HS side data in a wrong region.

It includes, from top to bottom, HIA data from LS side (ions in the 45° x 45° sector centred in the solar wind direction), HIA data from the high-sensitivity side (separately for four azimuthal sectors: ions arriving in the 90° x 180° sector with a field-of-view pointing in the sun, dusk, tail, and dawn direction respectively), omnidirectional CODIF data for H^+, He^+ and O^+ ions respectively, ion velocity components measured by HIA, and ion densities measured by HIA and by CODIF. Instrument operational mode and spacecraft telemetry mode data are also included, as well as spacecraft coordinates. As can be seen in the HIA mode panel, at the top, the instrument was initially in a solar wind - upstreaming ions mode (mode 3). The solar wind narrow-energy beam is clearly identified in the LS side HIA spectrogram, while at the same time the HS side HIA spectrogram for ions arriving from the sunward looking direction does not detect the solar wind beam. This is due to the energy-sweep scheme adopted during these modes, that stops (and "freezes") above the solar wind alpha particles energy, as explained in section 3.1. Some high-energy upstreaming ions are however visible at that time, in the high-sensitivity side HIA spectrograms, as well as in the CODIF H^+ spectrogram, which was then operating at the high-sensitivity side. Note that CODIF also does not detect the solar

wind beam, for the same reason: the energy-sweep scheme adopted during these modes (cf. Fig. 3.2), but solar wind beam data are supplied by HIA. At 12:40 UT the instrument, while in the solar wind, was switched into mode 12 (magnetosheath mode). Both instruments switched then to an omnidirectional full energy sweep scheme (cf. section 3.1), and the low-sensitivity side of HIA ceased collecting data. The solar wind beam became then detectable in the sunward looking direction spectrogram from the HIA high-sensitivity side (but with a lower energy resolution), and in the CODIF data, collected then from the high-sensitivity instrument side, but with a strong saturation in the solar wind beam energies. Note, however, the ability of the CODIF high-sensitivity side to detect the relatively weak fluxes of the upstreaming ion populations. The energy flux of these upstreaming ions is a factor of ~2000 lower than the energy flux of the solar wind beam ions, as this beam population is measured by the low-sensitivity side of HIA. At 14:40 UT the spacecraft entered in the magnetosheath, as revealed by the broader energy distribution of the detected ions (bow shock heating) and by the anisotropic flow shown in the four directional HIA spectrograms.

7 References

Blagau, A., I. Dandouras, A. Barthe, S. Brunato, G. Facskó, V. Constantinescu: In-flight calibration of Hot Ion Analyser onboard Cluster, Geosci. Instrum. Method, **3**, 49, doi:10.5194/gi-3-49-2014 (2014)

Daly, P.W., et al.: Users Guide to the Cluster Science Data System. DS–MPA–TN–0015 (2002)

Dandouras, I., V. Pierrard, J. Goldstein, C. Vallat, G. K. Parks, H. Rème, C. Gouillart, F. Sevestre, M. McCarthy, L. M. Kistler, B. Klecker, A. Korth, M. B. Bavassano-Cattaneo, P. Escoubet, A. Masson: Multipoint observations of ionic structures in the Plasmasphere by CLUSTER-CIS and comparisons with IMAGE-EUV observations and with Model Simulations. In: AGU Monograph: Inner Magnetosphere Interactions: New Perspectives from Imaging, **159**, 23-53, 10.1029/159GM03 (2005)

Dandouras, I., A. Barthe: Cluster Active Archive: Interface Control Document for CIS. CAA-CIS-ICD-000, http://caa.estec.esa.int/caa/ug_cr_icd.xml (2013).

Dandouras, I., A. Barthe, E. Penou, S. Brunato, H. Rème, L.M. Kistler, M.B. Bavassano-Cattaneo, A. Blagau, and the CIS Team: Cluster Ion Spectrometry (CIS) Data in the Cluster Active Archive (CAA). In: Proceeding of the Cluster Workshop and CAA School, Springer, p. 369-375, 2010.

Dandouras, I., A. Barthe, L.M. Kistler, A. Blagau: Calibration Report of the CIS Measurements in the Cluster Active Archive. CAA-EST-CR-CIS, http://caa.estec.esa.int/caa/ug_cr_icd.xml (2013)

Ganushkina, N. Yu., I. Dandouras, Y. Y. Shprits, J. Cao, Locations of Boundaries of Outer and Inner Radiation Belts as Observed by Cluster and Double Star, J. Geophys. Res., **116**, A09234, doi:10.1029/2010JA016376 (2011)

Harvey, C.C., A.J. Allen, F. Dériot, C. Huc, M. Nonon-Latapie, C.H. Perry, S.J. Schwartz, T. Eriksson, S. McCaffrey: Cluster Metadata Dictionary. CAA-CDPP-TN-0002 (2008)

Kistler, L. M., Cluster CODIF Calibration Report, Part III: TOF Peak Analysis, Mass Threshold and "Spillover" Determination, CAA Instrument Documents (2000)

Kistler, L. M., C. G. Mouikis, K. J. Genestreti: In-flight Calibration of the Cluster/CODIF sensor, Geosci. Instrum. Method, **2**, 225-235, doi:10.5194/gi-2-225-2013 (2013)

Laakso, H. , C. Perry, S. McCaffrey, D. Herment, A. J. Allen, C. C. Harvey, C. P. Escoubet, C. Gruenberger, M. G. G. T. Taylor and R. Turner, Cluster Active Archive: Overview, in The Cluster Active Archive - Studying the Earth's Space Plasma Environment, edited by Laakso et al., pp. 3-37, Springer (2010)

Laakso, H., Cluster Active Archive - User Guide, CAA-EST-UG-0001, http://caa.estec.esa.int/caa/instr_doc.xml (2012)

Martz, C., J.A. Sauvaud, H. Rème : Accuracy of ion distribution measurements and related parameters using the Cluster CIS experiment. In: Spatio-Temporal Analysis for Resolving Plasma Turbulence (START), ESA WPP-047, 229 (1993)

Perry, C., T. Eriksson, P. Escoubet, S. Esson, H. Laakso, S. McCaffrey, T. Sanderson, H. Bowen, A.Allen, C. Harvey: The ESA Cluster Active Archive. In: Proceeding of the Cluster and Double Star Symposium-5th Anniversary of Cluster in Space, ESA SP-598, Noordwjik (2006)

Prince, R.H., J.A. Cross: Gain Fatigue Mechanism in Channel Electron Multipliers. Rev. Sci. Instrum., **42**, 66; DOI:10.1063/1.1684879 (1971)

Rème, H., C. Aoustin, J.M. Bosqued, I. Dandouras, B. Lavraud, J.A. Sauvaud, A. Barthe, J. Bouyssou, Th. Camus, O. Coeur-Joly, A. Cros, J. Cuvilo, F. Ducay, Y. Garbarowitz, J.L. Medale, E. Penou, H. Perrier, D. Romefort, J. Rouzaud, C. Vallat, D. Alcaydé, C. Jacquey, C. Mazelle, C. dâUston, E. Möbius, L.M. Kistler, K. Crocker, M. Granoff, C. Mouikis, M. Popecki, M. Vosbury, B. Klecker, D. Hovestadt, H. Kucharek, E. Kuenneth, G. Paschmann, M. Scholer, N. Sckopke, E. Seidenschwang, C.W. Carlson, D.W. Curtis, C. Ingraham, R.P. Lin, J.P. McFadden, G.K. Parks, T. Phan, V. Formisano, E. Amata, M.B. Bavassano-Cattaneo, P. Baldetti, R. Bruno, G. Chionchio, A. Di Lellis, M.F. Marcucci, G. Pallocchia, A. Korth, P.W. Daly, B. Graeve, H. Rosenbauer, V. Vasyliunas, M. McCarthy, M. Wilber, L. Eliasson, R. Lundin, S. Olsen, E.G. Shelley, S. Fuselier, A.G. Ghielmetti, W. Lennartsson, C.P. Escoubet, H. Balsiger, R. Friedel, J-B. Cao, R. A. Kovrazhkin, I. Papamastorakis, R. Pellat, J. Scudder, B. Sonnerup: First multispacecraft ion measurements in and near the Earth's magnetosphere with the identical Cluster ion spectrometry (CIS) experiment. Ann. Geophys., **19**, 1303 (2001)

Torkar, K., W. Riedler, C.P. Escoubet, M. Fehringer, R. Schmidt, R.J.L. Grard, H. Arends, F. Rüdenauer, W. Steiger, B.T. Narheim, K. Svenes, R. Torbert, M. André, A. Fazakerley, R. Goldstein, R.C. Olsen, A. Pedersen, E. Whipple, H. Zhao: Active spacecraft potential control for Cluster implementation and first results. Ann. Geophys., **19**, 1289 (2001)

8 APPENDIX A: CIS DATASETS

The CIS datasets stored in the CAA are:

Dataset Id	Dataset Title
Ion Moments	
CP_CIS-HIA_ONBOARD_MOMENTS	Ion Moments
CP_CIS-CODIF_HS_H1_MOMENTS	H+ Moments (High sensitivity)
CP_CIS-CODIF_LS_H1_MOMENTS	H+ Moments (Low sensitivity)
CP_CIS-CODIF_HS_He1_MOMENTS	He+ Moments (High sensitivity)
CP_CIS-CODIF_LS_He1_MOMENTS	He+ Moments (Low sensitivity)
CP_CIS-CODIF_HS_O1_MOMENTS	O+ Moments (High sensitivity)
CP_CIS-CODIF_LS_O1_MOMENTS	O+ Moments (Low sensitivity)
CP_CIS-CODIF_He1_DENSITY_CORRECTED	Corrected He+ Density
Ion 1D omni-directional distributions	
CP_CIS-HIA_HS_1D	Ions 1D distribution (omni-directional, High sensitivity)
CP_CIS-HIA_LS_1D	Ions 1D distribution (omni-directional, Low sensitivity)
CP_CIS-CODIF_H1_1D	H+ 1D distribution (omni-directional)
CP_CIS-CODIF_He1_1D	He+ 1D distribution (omni-directional)
CP_CIS-CODIF_O1_1D	O+ 1D distribution (omni-directional)
Ion 2D pitch angle distributions	
CP_CIS-HIA_PAD_HS_MAG_IONS	Ion pitch angle distribution (High sensitivity)
CP_CIS-CODIF_PAD_HS_H1	H+ pitch angle distribution (High sensitivity)
CP_CIS-CODIF_PAD_LS_H1	H+ pitch angle distribution (Low sensitivity)
CP_CIS-CODIF_PAD_HS_He1	He+ pitch angle distribution (High sensitivity)
CP_CIS-CODIF_PAD_LS_He1	He+ pitch angle distribution (Low sensitivity)
CP_CIS-CODIF_PAD_HS_O1	O+ pitch angle distribution (High sensitivity)
CP_CIS-CODIF_PAD_LS_O1	O+ pitch angle distribution (Low sensitivity)
Ion 3D distributions	
CP_CIS-HIA_HS_MAG_IONS	Ion 3D distribution (High sensitivity, Magnetospheric mode)
CP_CIS-HIA_HS_SW_IONS	Ion 3D distribution (High sensitivity, Solar Wind mode)
CP_CIS-HIA_LS_SW_IONS	Ion 3D distribution (Low sensitivity, Solar Wind mode)
CP_CIS-CODIF_HS_H1	H+ 3D distribution (High sensitivity)
CP_CIS-CODIF_LS_H1	H+ 3D distribution (Low sensitivity)
CP_CIS-CODIF_HS_He2	He++ 3D distribution (High sensitivity)
CP_CIS-CODIF_LS_He2	He++ 3D distribution (Low sensitivity)
CP_CIS-CODIF_HS_He1	He+ 3D distribution (High sensitivity)
CP_CIS-CODIF_LS_He1	He+ 3D distribution (Low sensitivity)
CP_CIS-CODIF_HS_O1	O+ 3D distribution (High sensitivity)
CP_CIS-CODIF_LS_O1	O+ 3D distribution (Low sensitivity)
CP_CIS-CODIF_RPA_H1	H+ 3D distribution (RPA mode)
CP_CIS-CODIF_RPA_He2	He++ 3D distribution (RPA mode)
CP_CIS-CODIF_RPA_He1	He+ 3D distribution (RPA mode)
CP_CIS-CODIF_RPA_O1	O+ 3D distribution (RPA mode)

Ancillary	
CP_CIS-MODES	Instrument modes
CP_CIS-CODIF_CAVEATS	CODIF caveats
CP_CIS-HIA_CAVEATS	HIA caveats
CP_CIS-CODIF_H1_QUALITY	CODIF H+ quality indices
CP_CIS-CODIF_He1_QUALITY	CODIF He+ quality indices
CP_CIS-CODIF_He2_QUALITY	CODIF He++ quality indices
CP_CIS-CODIF_O1_QUALITY	CODIF O+ quality indices
CP_CIS-HIA_QUALITY	HIA quality indices
CP_CIS-CODIF_HS_RAT_IONS	Monitor Rates (High sensitivity)
CP_CIS-CODIF_LS_RAT_IONS	Monitor Rates (Low sensitivity)
CP_CIS-CODIF_HS_SEL	Time of Flight selected events (High sensitivity)
CP_CIS-CODIF_LS_SEL	Time of Flight selected events (Low sensitivity)
CP_CIS-CODIF_HS_64M_IONS	Ion 3D distribution, 64 m/q ranges (High sensitivity)
CP_CIS-CODIF_LS_64M_IONS	Ion 3D distribution, 64 m/q ranges (Low sensitivity)
Graphical	
CG_CIS_SPECTRO	Ion spectrograms and moments plots
CSDS Prime and Summary Parameters	
PP_CIS	Preliminary ion parameters (spin resolution)
SP_CIS	Preliminary ion parameters (1 minute resolution)

9 APPENDIX B: CIS DATA QUALITY FLAGS

The following table gives a list of the **CIS-specific flags (caveats_keys)**, which are **included in the CIS data quality indices datasets** and appear when the data quality is inadequate, i.e. when a data quality index has a value less than 3 (cf. section 5.6). A description of the relevant caveats is given in section 6.2, including examples of data affected by these issues.

Quality index values, given in the table, correspond to the value set by the caveat key described in the same line of the table. However, for a given time, the quality index value given to the data might be lower, if several caveat keys simultaneously apply: the quality index value is then set to the lower of all, and all the applicable then caveat_keys are given in textual form.

Boxes are in grey when the corresponding instrument (CODIF or HIA) is not concerned by the given caveat.

Note: At the time of this writing (June 2017) the limitations related to a magnetospheric region - CIS mode mismatch have not yet been included in the CIS data quality datasets delivered to the CAA. They will be included in the near future.

Flag (caveats_key)	Data Caveat	CODIF Quality Index				HIA Quality Index			
		3D	PAD	1D	Moments	3D	PAD	1D	Moments
Limitations related to operation incidents or scheduled special operations									
DISCRI	Wrong HIA discriminator levels					2	2	2	2
MCP	Wrong HIA MCP HV level					1	1	1	1
MCP	Wrong CODIF MCP HV level	1	1	1	1				
MCP_DC	HIA MCP HV discharge					1	1	1	1
MCP_DC	CODIF MCP HV discharge	1	1	1	1				
PACC_DC	CODIF post-acceleration HV discharge	1	1	1	1				
TM	Instrument-spacecraft telemetry rate mode mismatch	1	1	1	1	1	1	1	1
CALIB	CODIF onboard calibrations	1	1	1	1				
CALIB	HIA onboard calibrations					1	1	1	1
RESET	Instrument reset	-1	-1	-1	-1	-1	-1	-1	-1
NO_DATA	CIS OFF or in mode 7 or 15	0	0	0	0	0	0	0	0
ANL_OFF	Electrostatic analyser OFF (e.g. 2012 HIA analyser incidents)					0	0	0	0
ECLIPSE	Eclipse	1	-1	3	1	-1	-1	-1	-1
PACKET	Incomplete CODIF TM packets	1 (for the concerned dataset)							
PACKET	Incomplete HIA TM packets					1 (for the concerned dataset)			
ONBOARD_BUG	Meaningless data due to an onboard processing bug					-1 (for the concerned dataset)			

NO_LS_DATA	CODIF LS data not provided on spacecraft C1 and C3 (used for instrument test only)	0	0	0	0	

Flag (caveats_key)	Data Caveat	CODIF Quality Index				HIA Quality Index			
		3D	PAD	1D	Moments	3D	PAD	1D	Moments
Limitations related to the sampling of the ion distributions									
LOW_COUNTS	Poor CODIF counting statistics	2	2	3	2				
LOW_COUNTS	Poor HIA counting statistics					2	2	3	2
SC_POT	High spacecraft potential	3	3	3	2	3	3	3	2
HE2	He^{++} contamination from H^{+}	1	1	1	1				
O1	O^{+} contamination when high H^{+} fluxes	1	1	1	1				
DEF_ANODES	CODIF on sc3 deficient anodes	1	1	2	1				
GYRORAD	Finite gyroradius / gyroperiod effects or FGM calibration	3	2	3	3	3	2	3	3
Limitations related to a magnetospheric region - CIS mode mismatch									
SW_MODE	Magnetosheath or magnetosphere when CIS is in a solar wind mode	1	-1	1	-1	1	-1	1	-1
SW_HS	Solar wind mode & CODIF on HS	1	-1	1	-1				
MSH_HS	Mode 12 or 14 & CODIF on HS (for data after 1 Nov, 2003)	1	-1	1	-1				
MAG_MODE	Solar wind when CIS is in a magnetospheric mode	2	2	2	2	2	2	2	2
RAD_BELT	Radiation Belts background (does not concern cleaned CODIF datasets)	1	1	2	1	1	1	1	-1

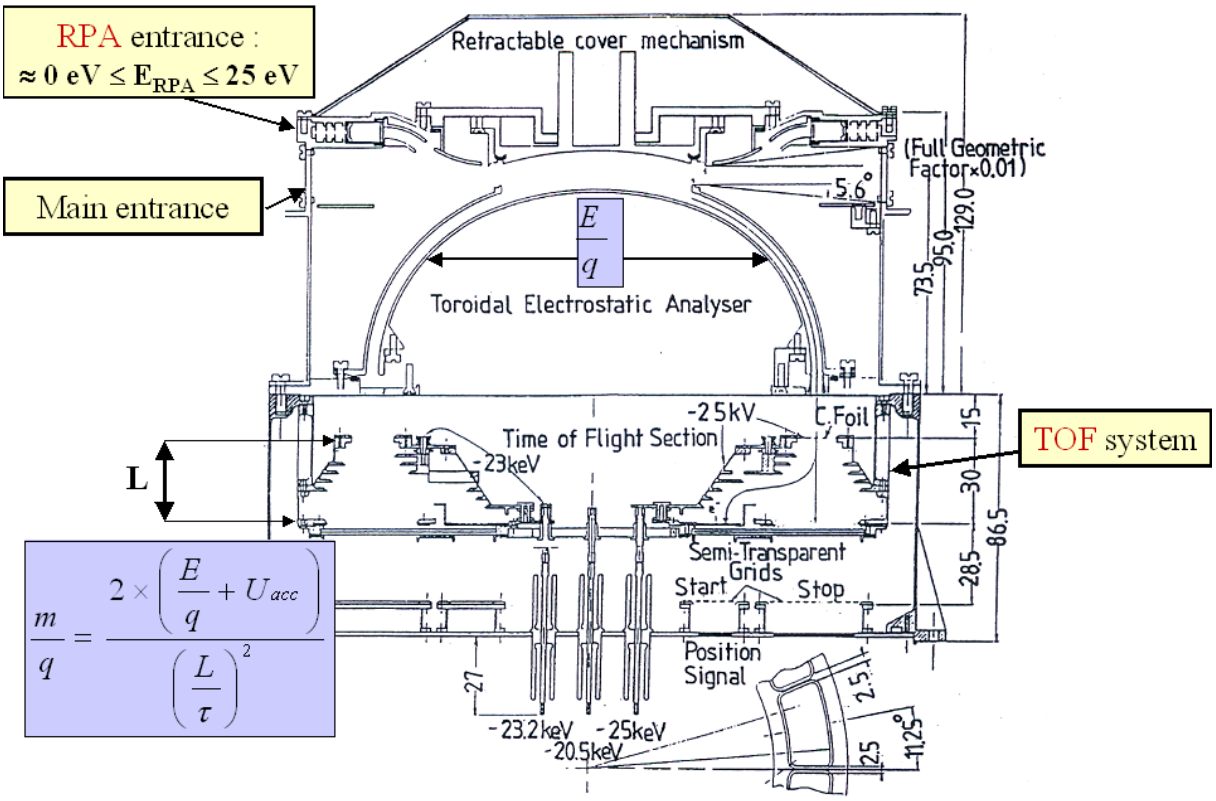

Figure 2.1

Schematic of the CODIF instrument

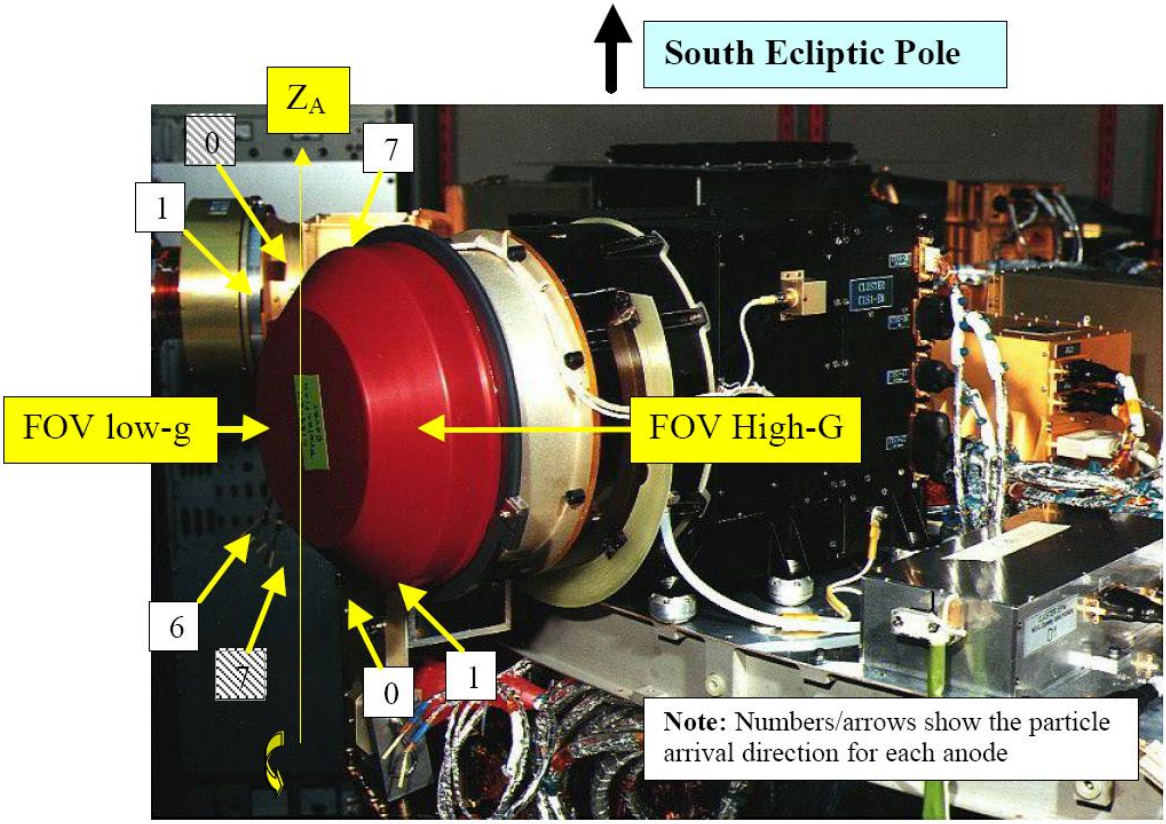

Figure 2.2

Schematic of the CIS-1 (CODIF) anodes field of view (High-G / low-g), with respect to the main axes. In grey are the two "blind" anodes (not used for data collection).

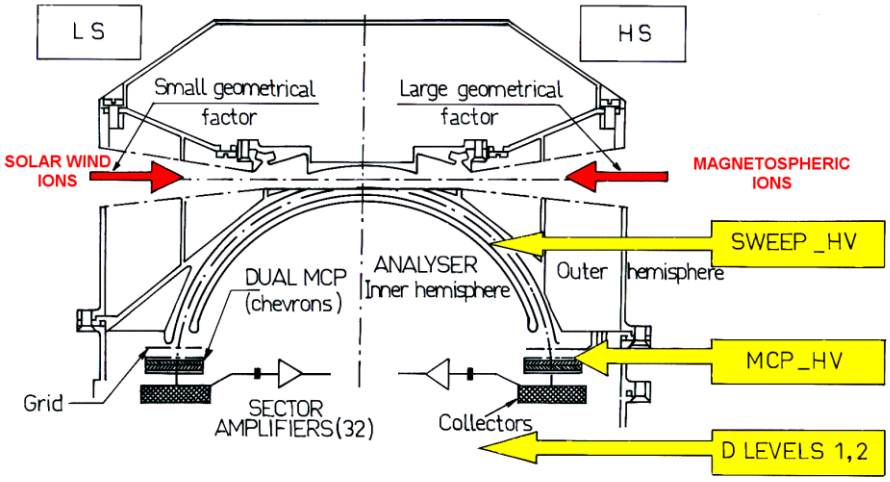

Figure 2.3

Cross sectional view of the HIA instrument.

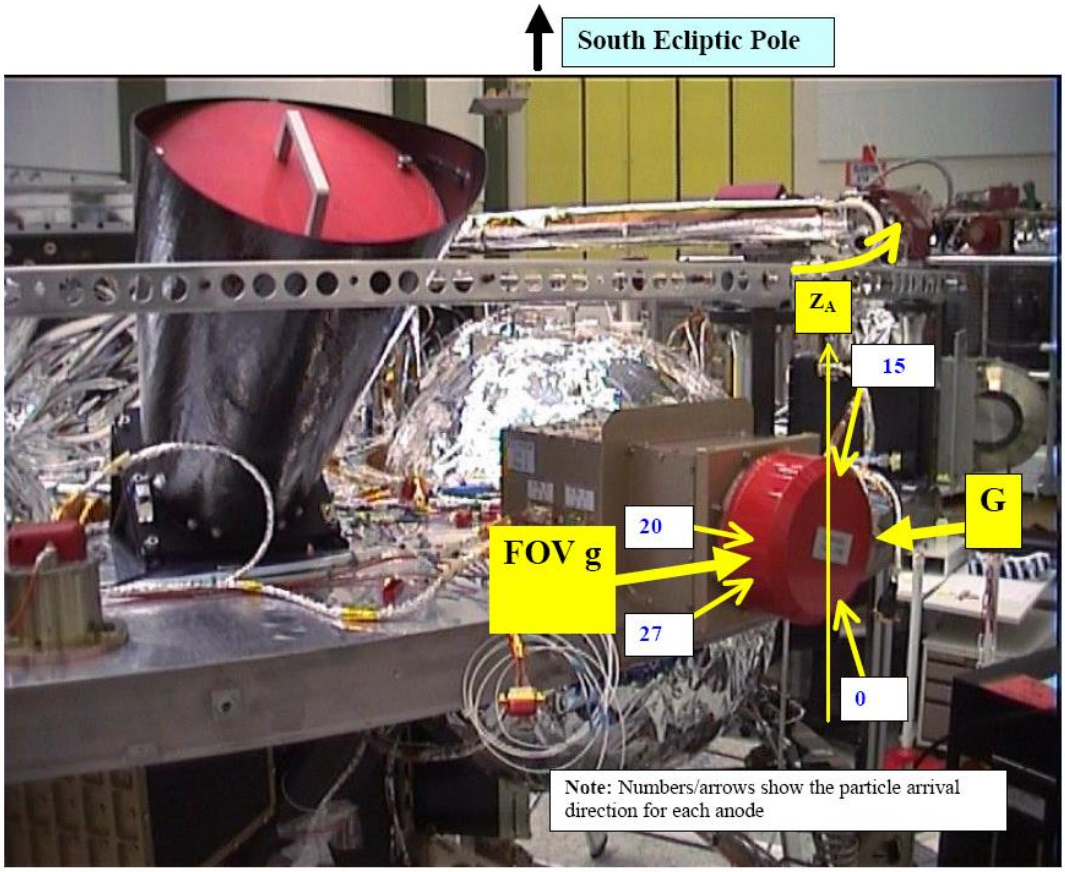

Figure 2.4

Schematic of the CIS-2 (HIA) anodes field of view (High-G / low-g), with respect to the main axes.

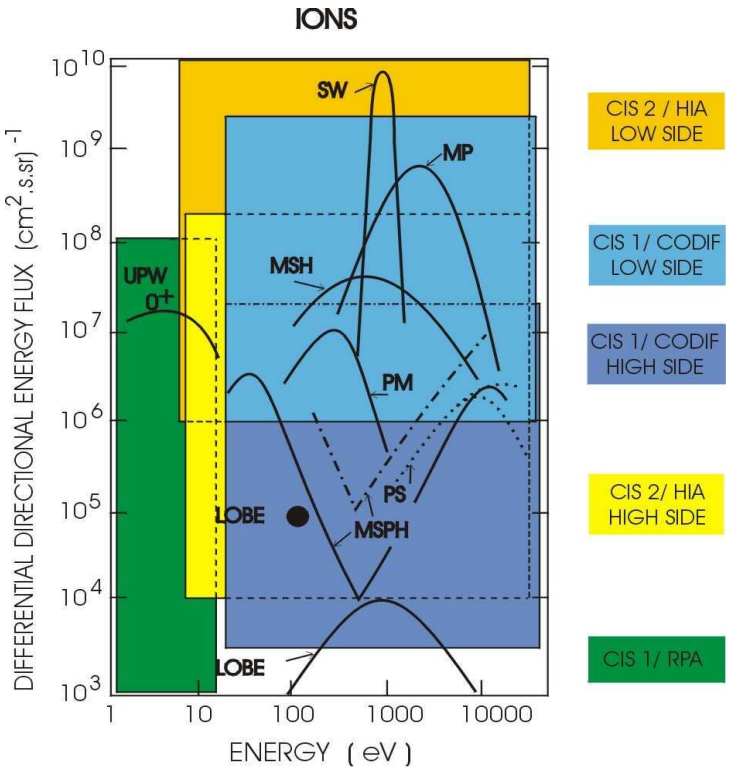

Figure 2.5

Representative ion fluxes encountered along the Cluster orbit in the solar wind (SW), the magnetopause (MP), the magnetosheath (MSH), the plasma mantle (PM), the plasma sheet (PS), the lobe and upwelling ions (UPW). The range of the different sensitivities of CIS1/CODIF (Low Side, High Side and RPA) and CIS2/HIA (Low Side and High Side) are shown with different colours.

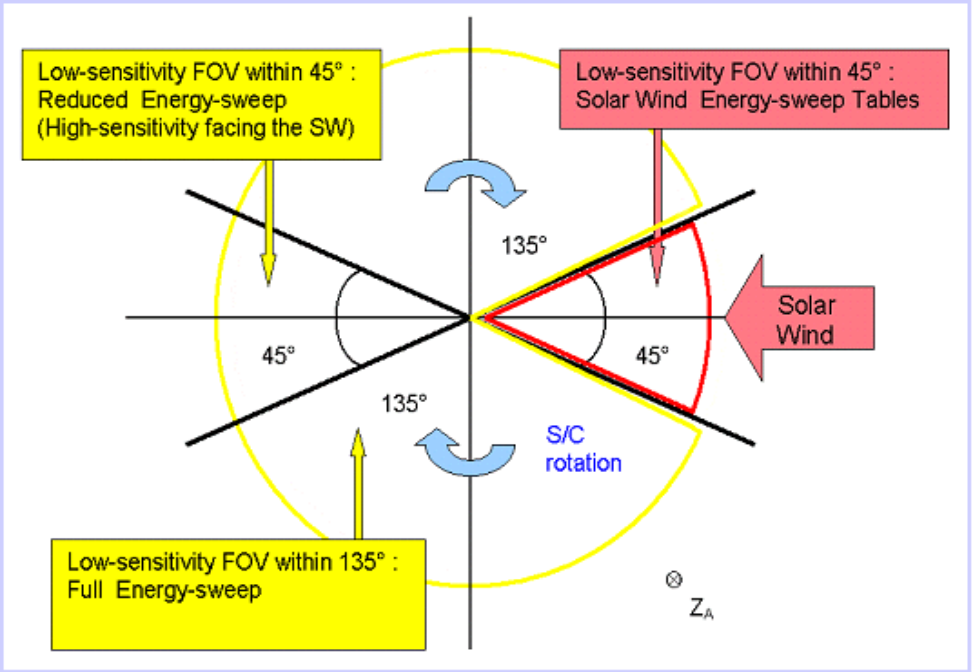

Figure 3.1

Schematic of the CIS-2 (HIA) energy-sweep scheme, as a function of the instrument field-of-view orientation in the spin plane (solar wind modes 0-5).

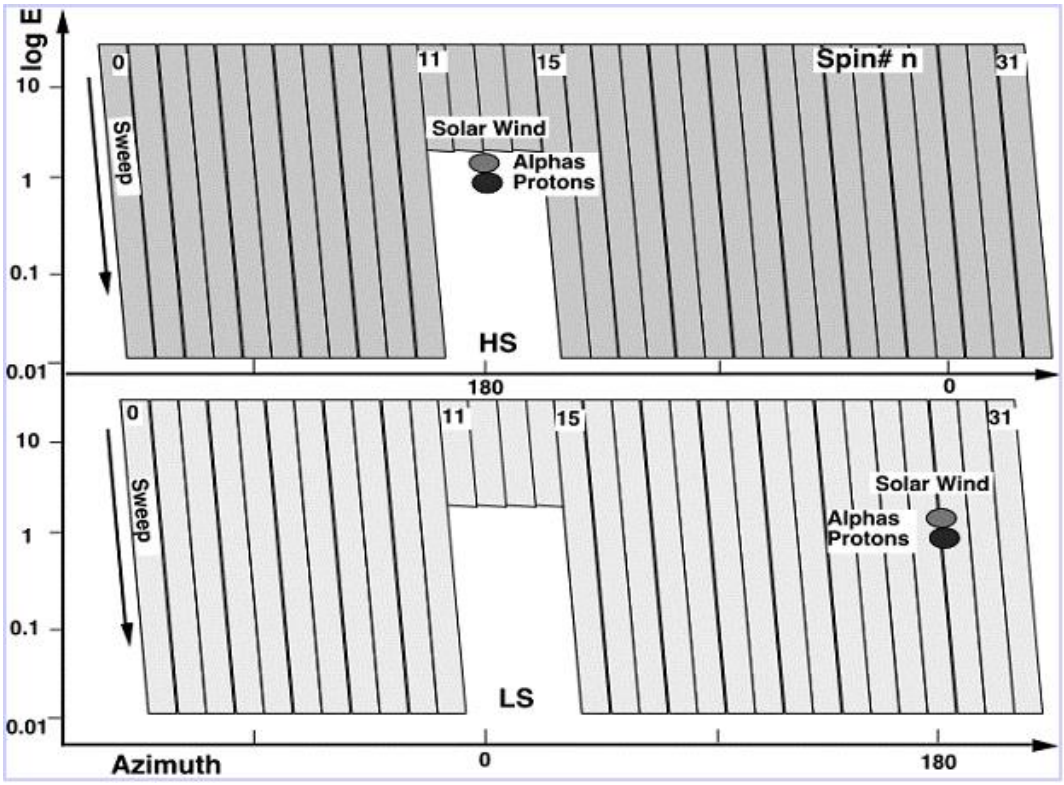

Figure 3.2

Schematic of the CIS-1 (CODIF) energy-sweep scheme, for solar wind modes, as a function of the spin phase: "high G" *field-of-view orientation (upper panel,) and* "low g" *field-of-view orientation (bottom panel). The energy "freeze", during the reduced energy sweeps, is at about 2 keV.*

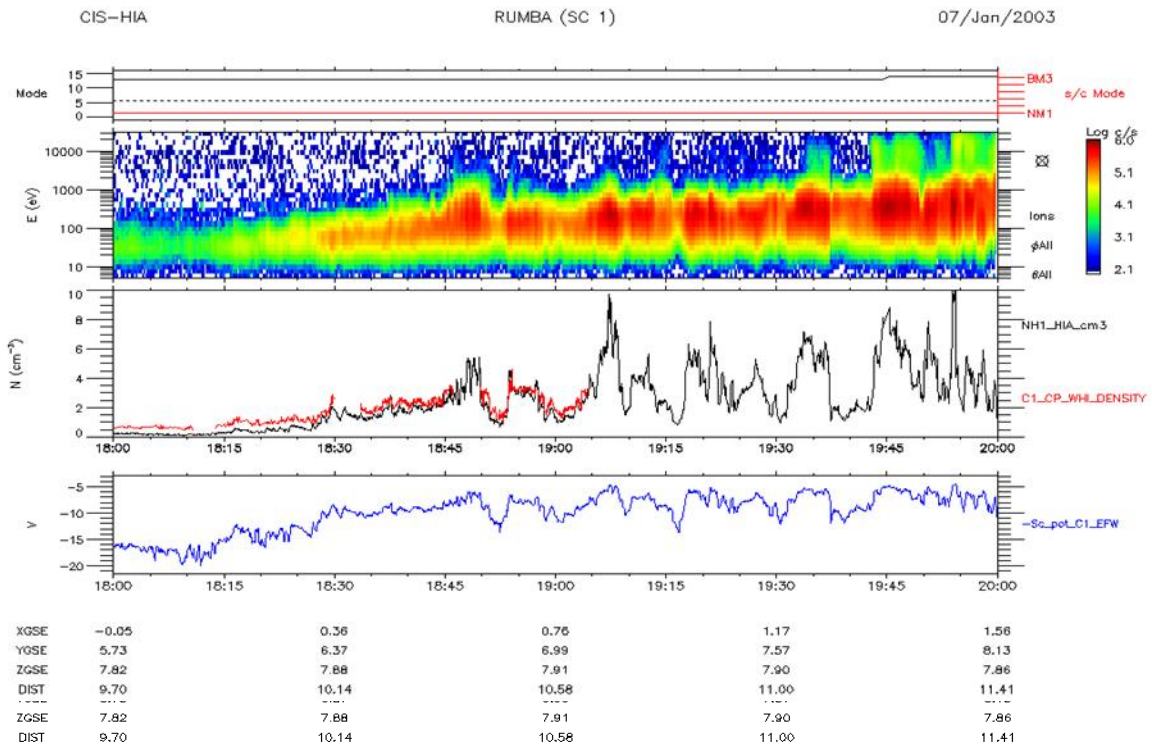

Figure 6.1

Example of HIA energy-time spectrogram and HIA - WHISPER density comparison in the cusp. HIA density plot in black, and WHISPER provided density plot in red. In blue is the negative of the spacecraft potential, measured by the EFW experiment. Notice the deviation between the density values provided by the two instruments before ~18:30 UT, when spacecraft charging is stronger in this low-density region. WHISPER data courtesy of the WHISPER team and the CAA. EFW data courtesy of the EFW team and the CAA.

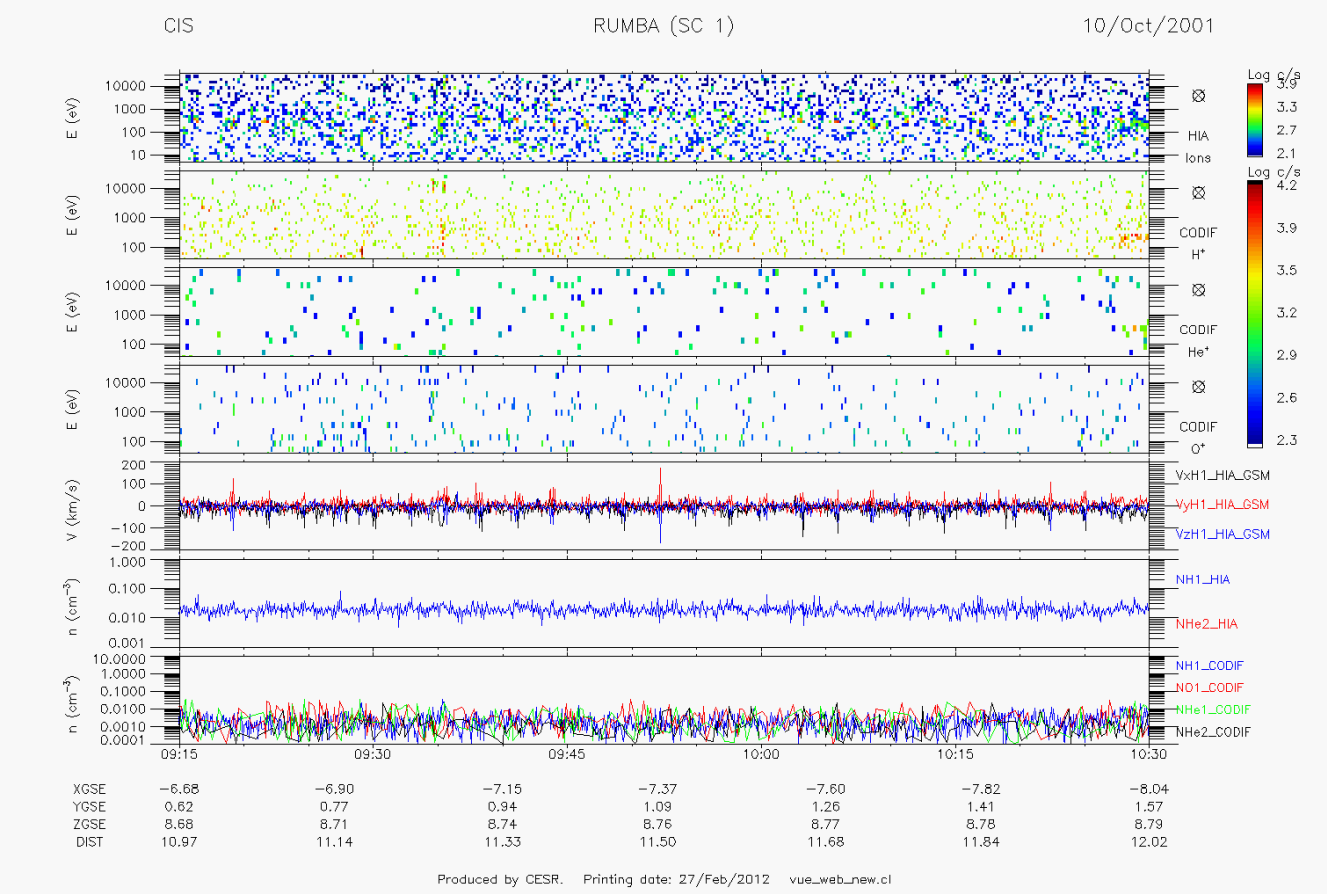

Figure 6.2

Example of very poor HIA (top spectrogram) and CODIF (next 3 spectrograms) counting statistics, in the magnetotail lobe. The effects of these poor counting statistics in the ion moments are shown in the bottom 3 panels (noisy data).

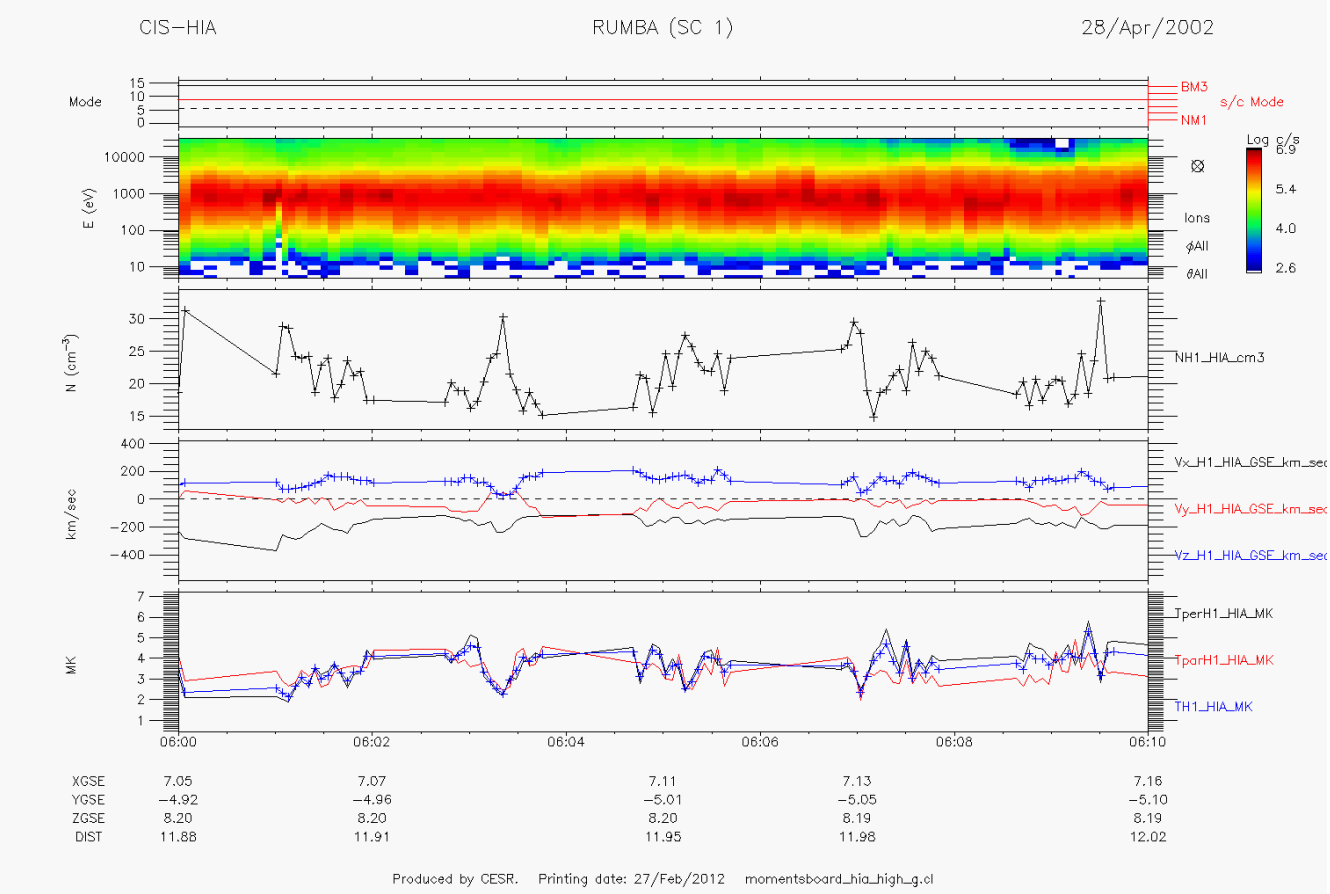

Figure 6.3

Example of partially transmitted HIA data. The effect is clear in the ion moments, where two successive measurements appear separated by as much as 1 minute, due to data loss between them.

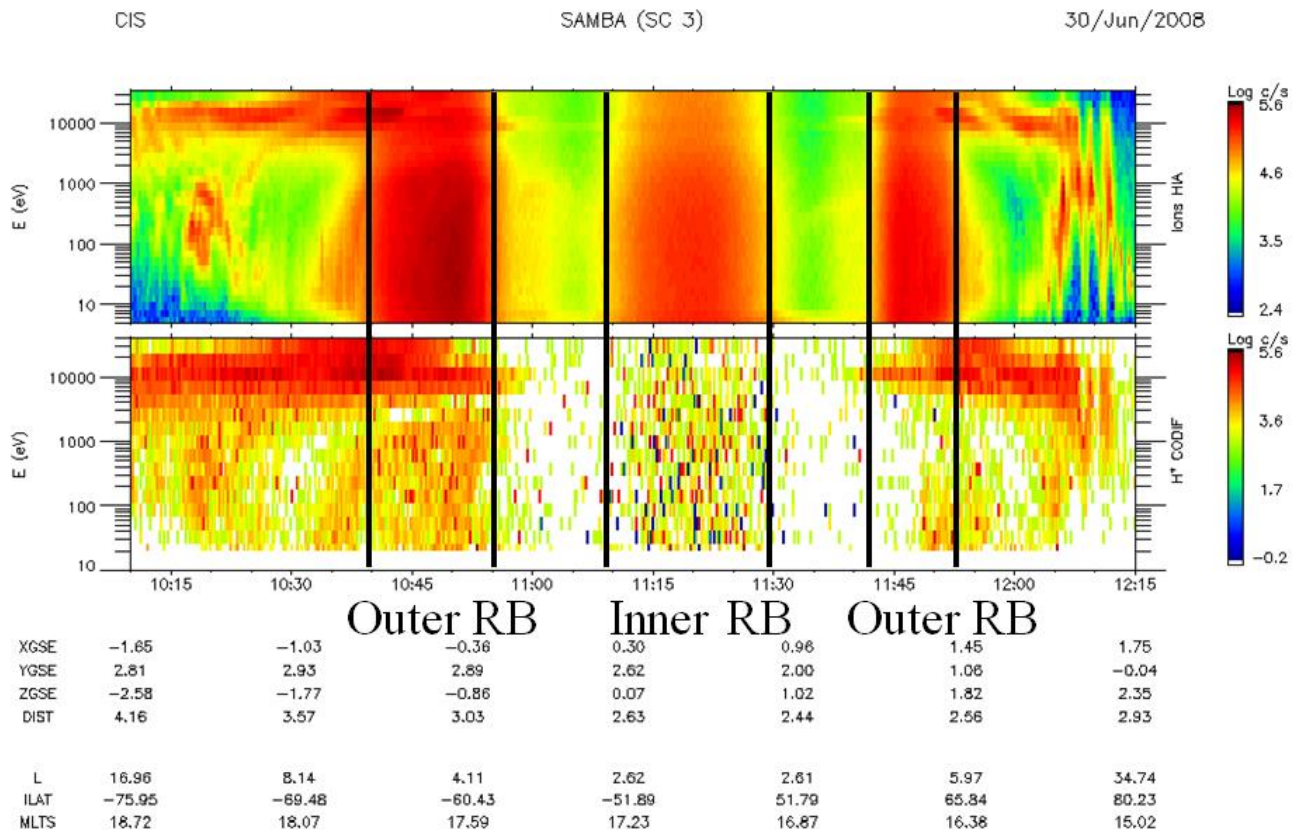

Figure 6.4.a

Example of background induced on the HIA (top panel) and CODIF (bottom panel) ion counting statistics, due to penetrating particles from the radiation belts.

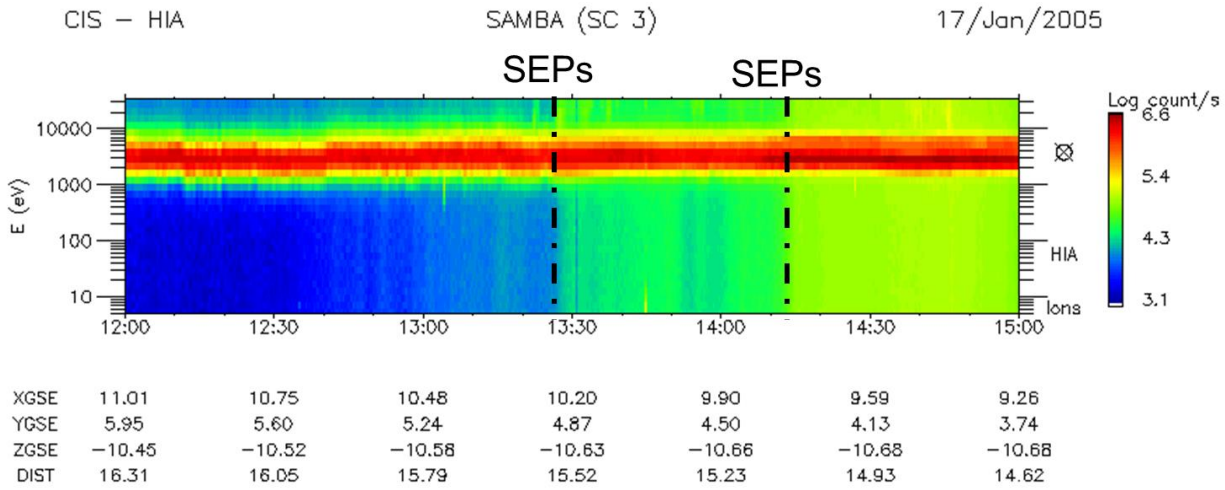

Figure 6.4.b

Example of background induced on the HIA ion counting statistics, while in the solar wind, due to the arrival of Solar Energetic Particles (SEPs) during an extreme solar event.

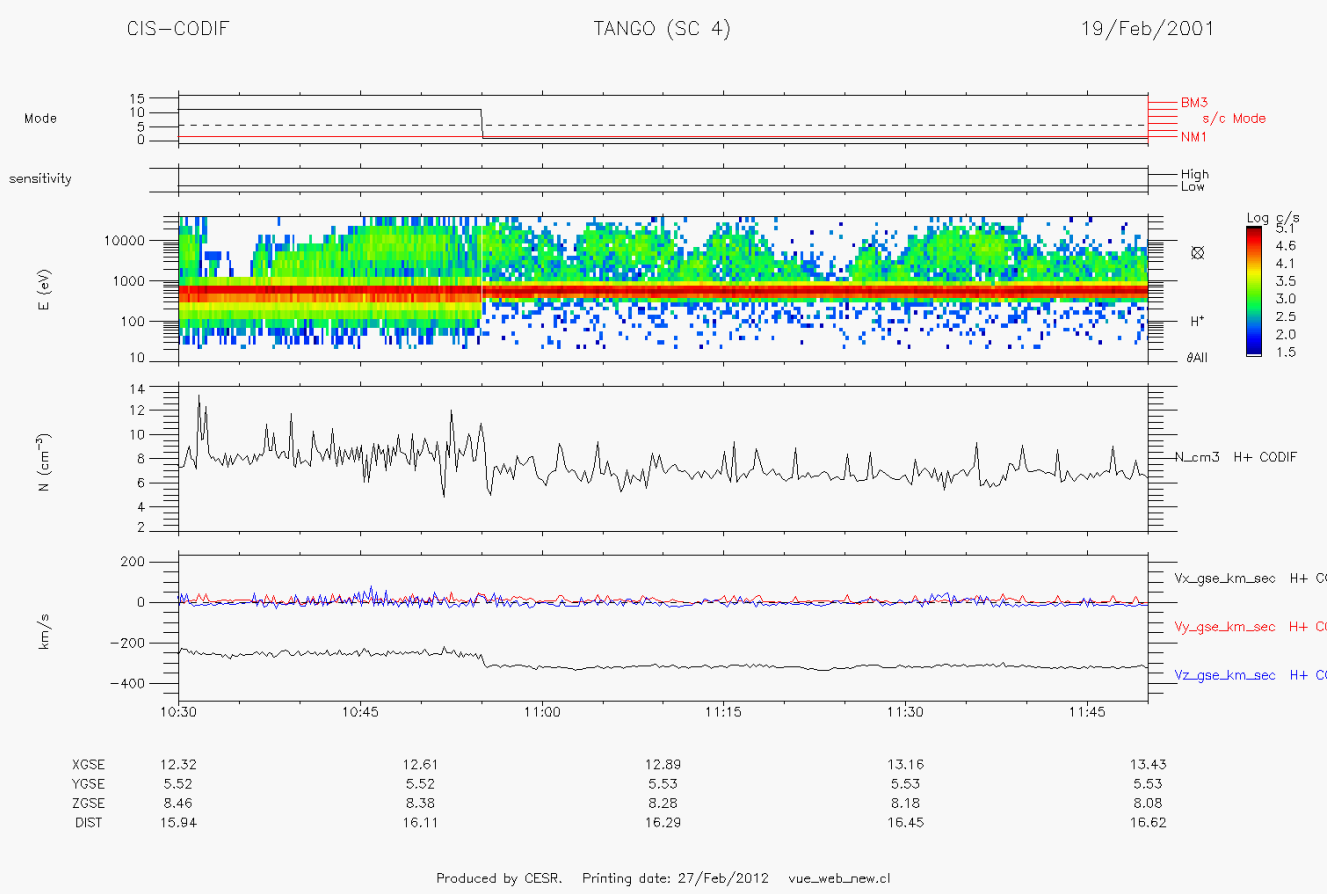

Figure 6.5

Example of CODIF cross-talk in the solar wind, while in a magnetospheric mode. The switch from a magnetospheric to a solar wind mode occurred at 10:55 UT. The cross-talk results in an increased density and in a reduced absolute value of the V_x component of the velocity.

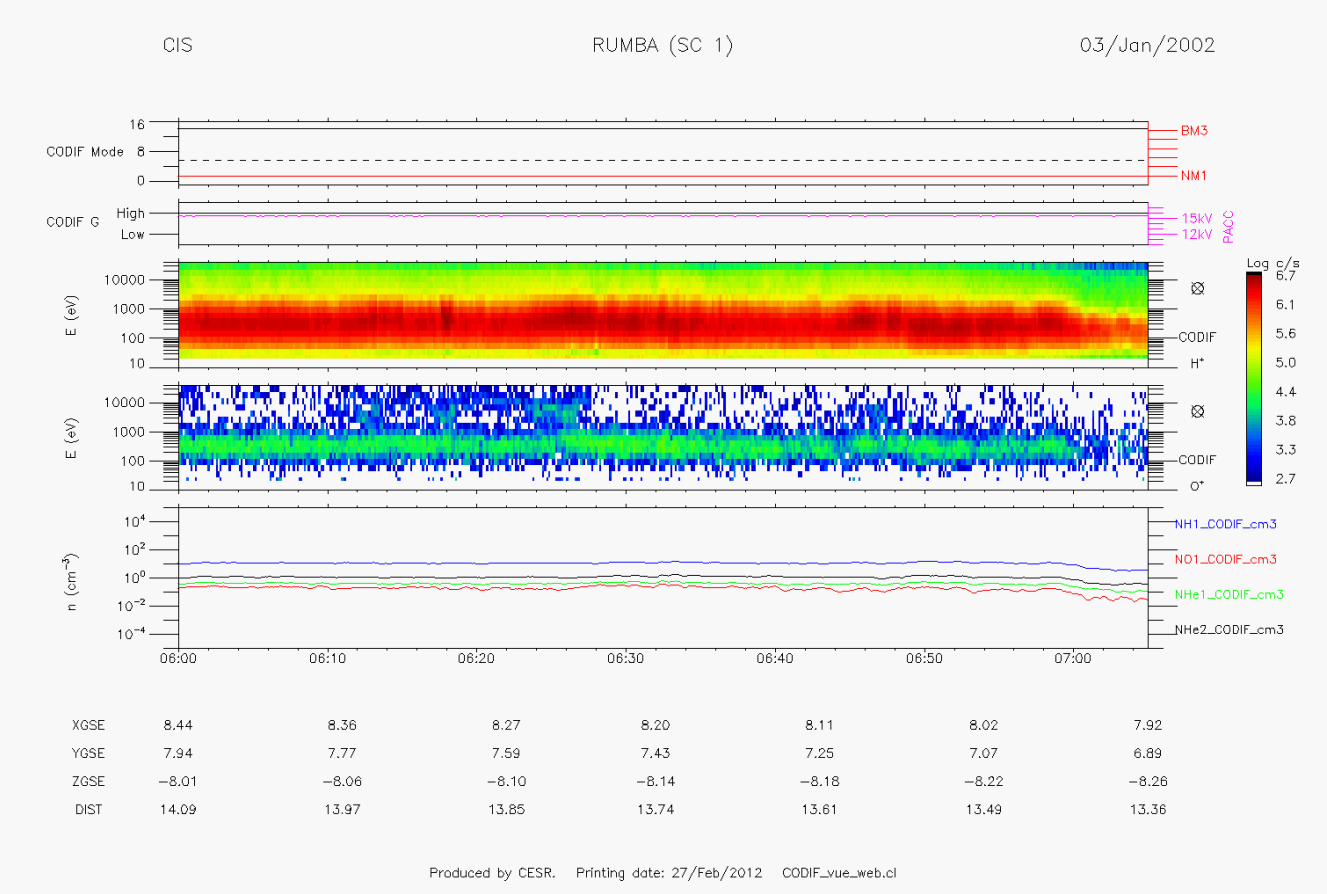

Figure 6.6

Example of CODIF O^+ data contamination from very high H^+ fluxes in the magnetosheath. The faint green pattern in the O^+ data, between ~100 and ~1000 eV, is a "ghost image" of this H^+ contamination. At the same time, high-energy (~10 000 eV) O^+ fluxes, observed around 06:25 UT, are "real" O^+ (no H^+ high-flux counterpart).

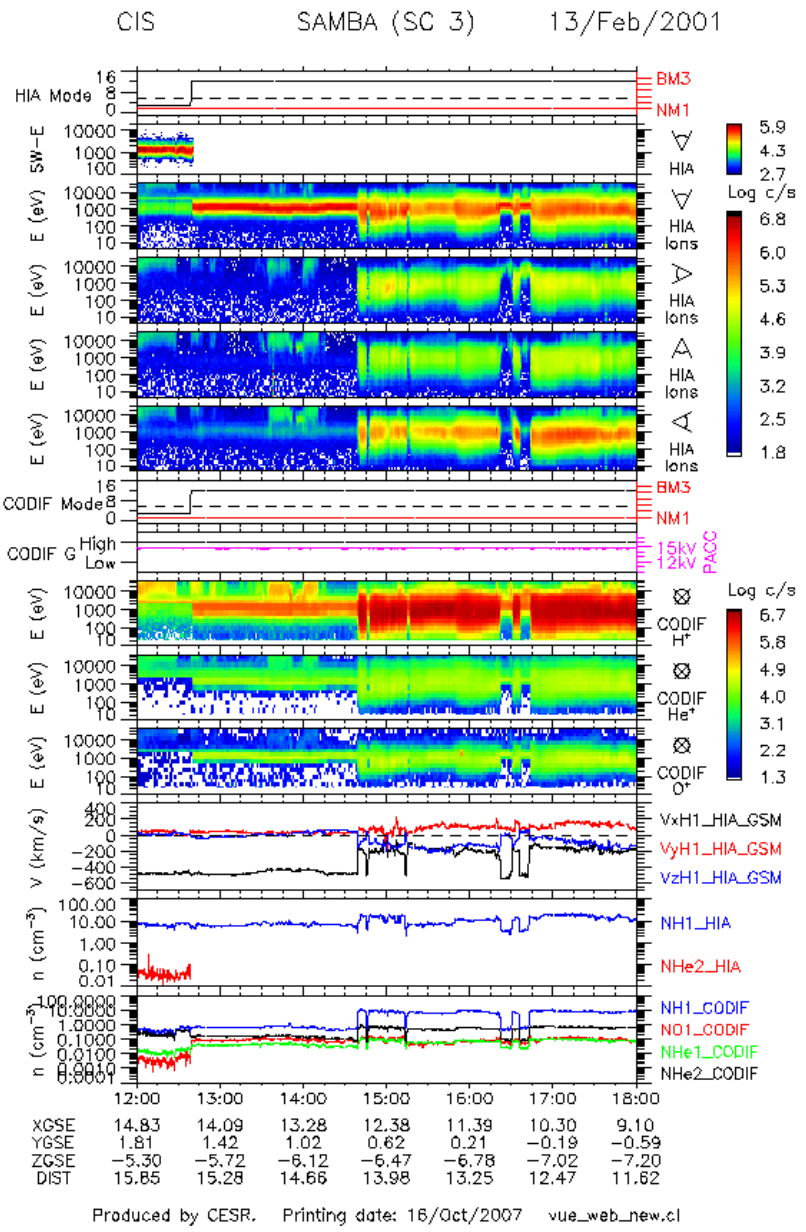

Figure 6.7

CIS energy-time spectrogram, illustrating the influence that can have on the data an inappropriate mode selection. See text for details.